Toxicology Letters 243 (2016) 67–77

Contents lists available at ScienceDirect

Toxicology Letters

journal homepage: www.elsevier.com/locate/toxlet

Disturbance of ion environment and immune regulation following biodistribution of magnetic iron oxide nanoparticles injected intravenously

Eun-Jung Park[a,*], Sang-Wook Kim[b], Cheolho Yoon[c], Younghun Kim[d], Jong Sung Kim[e]

[a] Myunggok Eye Research Institute, Konyang University, Daejeon 302-718, South Korea
[b] Department of Molecular Science and Technology, Ajou University, Suwon 443-749, South Korea
[c] Seoul Center, Korea Basic Science Institute, Seoul 126-16, South Korea
[d] Department of Chemical Engineering, Kwangwoon University, Seoul 139-701, South Korea
[e] Department of Community Health and Epidemiology, Faculty of Medicine, Dalhousie University, Halifax, Canada

HIGHLIGHTS

- In this study, we used magnetic iron oxide nanoparticles (M-FeNPs).
- Mice received a single injection of M-FeNPs via the tail vein.
- At 13 weeks post-injection, M-FeNPs the most distributed in the spleen.
- M-FeNPs altered levels of redox response-related elements in tissues.
- M-FeNPs disturbed ion homeostasis in tissues.
- M-FeNPs attenuated expression of antigen presentation-related proteins.

ARTICLE INFO

Article history:
Received 2 October 2015
Received in revised form 12 November 2015
Accepted 30 November 2015
Available online 11 December 2015

Keywords:
Iron oxide nanoparticles
Magnetite
Distribution
Ion environment
Immunotoxicity

ABSTRACT

Although it is expected that accumulation of metal oxide nanoparticles that can induce redox reaction in the biological system may influence ion homeostasis and immune regulation through generation of free radicals, the relationship is still unclear. In this study, mice received magnetic iron oxide nanoparticles (M-FeNPs, 2 and 4 mg/kg) a single via the tail vein, and their distribution in tissues was investigated over time (1, 4, and 13 weeks). In addition, we evaluated the effects on homeostasis of redox reaction-related elements, the ion environment and immune regulation. The iron level in tissues reached at the maximum on 4 weeks after injection and M-FeNPs the most distributed in the spleen at 13 weeks. Additionally, levels of redox reaction-related elements in tissues were notably altered since 1 week post-injection. While levels of K^+ and Na^+ in tissue tended to decrease with time, Ca^{2+} levels reached to the maximum at 4 weeks post-injection. On 13 weeks post-injection, the increased percentages of neutrophils and eosinophils, the enhanced release of LDH, and the elevated secretion of IL-8 and IL-6 were clearly observed in the blood of M-FeNP-treated mice compared to the control. While expression of antigen presentation related-proteins and the maturation of dendritic cells were markedly inhibited following distribution of M-FeNPs, the expression of several chemokines, including CXCR2, CCR5, and CD123, was enhanced on the splenocytes of the treated groups. Taken together, we suggest that accumulation of M-FeNPs may induce adverse health effects by disturbing homeostasis of the immune regulation and ion environment.

1. Introduction

The Organization for Economic Co-operation and Development (OECD) established the OECD Working Party on Manufactured Nanomaterials to promote international co-operation on the human health and environmental safety aspects of manufactured

* Corresponding author at: Myunggok Eye Research Institute, Konyang University, 685, Gasuwon-dong, Seo-Gu, Daejeon, 302-718, South Korea.
E-mail address: pejtoxic@hanmail.net (E.-J. Park).

http://dx.doi.org/10.1016/j.toxlet.2015.11.030
0378-4274/

nanoparticles in 2006, and at its 7th meeting, it listed 13 high-priority nanomaterials for study (www.oecd.org., 2010). Among them, magnetic iron oxide nanoparticles (M-FeNPs) are attracting considerable interest in medical fields with objectives, such as a contrast agent of magnetic resonance imaging, drug delivery, and hyperthermia of cancer (Antonelli et al., 2013; Rosen et al., 2012; Wahajuddin and Arora, 2012; Sun et al., 2011; Hilger and Kaiser, 2012).

Nanoparticles exhibit different physical, chemical, optical, electrical, catalytic, and mechanical properties with the larger particles due to their unique manufacturing process, and their behavior, distribution, persistence, and bioaccumulation in humans depend on their interactions with human body components (Hagens et al., 2007; Monopoli et al., 2012; Nel et al., 2009; Sayes et al., 2007; Wittmaack, 2007; Yang et al., 2015). For example, on entering the bloodstream, nanoparticles can interact with blood components such as proteins, platelets, and red and white blood cells, and their effects within biological systems may be altered remarkably by the formation of the protein corona. In addition, some researchers suggested that nanoparticles were observed inside red blood cells (RBC) despite the fact that erythrocytes do not have phagocytic receptors (Geiser et al., 2005; Rothen-Rutishauser et al., 2006). This means that nanoparticles be able to cross the cell membrane via another process, such as electrostatic attraction or ion channels, as well a general foreign body uptake process, such as phagocytosis and endocytosis.

The applications of nanoparticles in medicine can represent another exposure route for nanoparticles besides typical exposure pathways, including inhalation, oral, and the skin (Yah et al., 2012). For example, nanoparticles can be injected directly into the body to enhance the contrast in medical imaging or for drug delivery applications, and wear from implanted biomaterials can inadvertently occur in the body (Shinohara et al., 2014; Wang et al., 2009). Additionally, the toxicity of nanoparticles depends on the internal dose (the dose of nanoparticles that reaches the systemic circulation and organs and tissues) rather than the external dose (the total dose of nanoparticles applied via typical exposure pathways) (Hagens et al., 2007; Braakhuis et al., 2014; Oberdörster et al., 2005). Therefore, identification of the target organ for accumulation is essential for the safe and reliable use of nanotechnology in consumer products, food, medicine, and other applications. In this regard, the liver and spleen have been identified as target organs of intravenously injected nanoparticles in some studies, and macrophages have been indicated as the key player in systemic circulation and for biodistribution of nanoparticles (Baratli et al., 2014; Fraga et al., 2014; Fujihara et al., 2015; Fabian et al., 2008; Yang et al., 2015), although a part of the individual nanoparticles can move freely within the body (Park et al., 2014a,b). Furthermore, some researchers recently reported an immunotoxic response following exposure to nanoparticles (Seydoux et al., 2014; Tkach et al., 2013; Altaf and Revell, 2013; Park et al., 2015). However, it remains unclear whether bioaccumulation in these tissues contributes directly to the immunotoxic response observed. Additionally, metal oxide nanoparticles can interact with receptors on the membrane repeating redox reactions in the body (Liu et al., 2006; Park et al., 2014c), in this process, metal oxide nanoparticles can influence the absorption and excretion of trace elements in the body. Furthermore, some metal oxide nanoparticles can be dissolved and ionized in our body, therefore we can guess that metal oxide nanoparticles may affect the intracellular ion environment in our body (Utembe et al., 2015). However, to date, there are very few reports on the effect of nanoparticles on the ion environment in vivo. Herein, we hypothesized that accumulation of M-FeNPs may induce adverse health effects by disturbing homeostasis in the function of immune system and ion environment. For this, we injected a single M-FeNPs (2 and 4 mg/kg) via the tail vein of mice considering that a 20 mg/kg dose is toxic for humans (Velez and Delaney, 2006; Yang et al., 2015), and then investigated biodistribution with time. In addition, we identified changes in the immune regulation and ion homeostasis following tissue accumulation of M-FeNPs.

2. Material and methods

2.1. Preparation and characterization of M-FeNPs

As described previously, M-FeNPs were manufactured by thermal decomposition method of precursors in the organic phase (Park et al., 2014a,b). Briefly, M-FeNPs, 2 mmol iron oleate, 1 mmol oleic acid, and 10 g 1-octadecene (Sigma–Aldrich, St. Louis, MO, USA) were loaded into a 50 mL, 3-necked flask and degassed under vacuum conditions at 100 °C for 1 h (Park et al., 2004). The temperature was raised to 320 °C, and the mixture was stirred for 30 min under an N_2 atmosphere prior to cooling to room temperature (RT). Iron oxide nanocrystals were precipitated from the reaction solution by adding isopropanol and were separated by centrifugation. Nanocrystals were dispersed in tetrahydrofuran (THF), followed by the addition of phospholipid. After evacuation of THF, the mixture was incubated at 50 °C under vacuum conditions for 10 min. Water was added, and unbound phospholipid was eliminated by dialysis. The same steps were performed without iron compounds for the vehicle control. M-FeNPs were spherical type (Supple 1). The surface charge on M-FeNPs prepared and suspended in FBS was -36.8 ± 2.3 and -9.4 ± 0.02 mV,

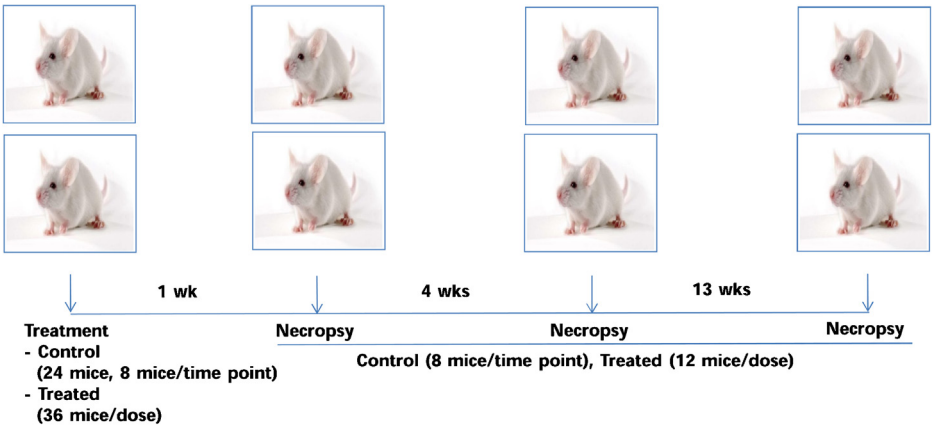

Fig. 1. An experimental design.

respectively, and their hydrodynamic diameter was 43.9 ± 3.7 and 37.0 ± 2.7 nm, respectively.

2.2. Animal care and M-FeNPs treatment

Six-week-old male ICR mice (26–28 g, OrientBio, Seongnam, Korea) were acclimatized for 1 week before beginning the study at a constant temperature of 23 ± 3 °C, relative humidity of 50 ± 10%, a 12 h light/dark cycle with a light intensity of 150–300 lx, and ventilation of 10–20 times/h. After acclimation, M-FeNPs (stock solution concentration: 3111.8 μg/mL), were injected into tail veins of restrained mice according to standard operating procedure for intravenous injection of Korea Institute of Toxicology, a good laboratory practice institute of Korea (2 and 4 mg/kg, control group: 8 mice/time point, treated group: 12 mice/group). The mice were euthanized on 1-, 4-, and 13-weeks after a single injection. The protocol for this experiment (IACUC No. 2012-0009) was assessed by the Institutional Animal Care and Committee (IACUC) of Ajou University (Suwon, Korea) and performed in accordance with the "Guide for the Care and Use of Laboratory Animals", an Institute for Laboratory Animal Research publication.

2.3. In vivo sample preparation and hematological analysis

The blood and tissues (the brain, thymus, lung, heart, liver, kidney, spleen, and testis) were collected on 1-, 4-, and 13-weeks after a single injection (Fig. 1). The blood was collected from the saphenous vein, and a part of the whole blood was centrifuged at 3000 rpm for 10 min to obtain serum for cytokine and lactate dehydrogenase (LDH) assay. Hematological analysis was performed using a blood autoanalyzer (HemaVet850, CDC Tech. Co., USA) at the Neodin Veterinary Science Institute (Seoul, Korea), a company specializing in this technology.

2.4. Trace elements and ion concentration measurement

Tissues (half of the brain, heart and spleen, whole of the thymus, a part of the lung and liver (0.5–0.8 g), and left piece of the kidney and testis) and blood (150 μL) were digested in a mixture of HNO_3 (70%, 7 mL) and H_2O_2 (35%, 1 mL) solution using a microwave digestion system (Milestone, Sorisole, Italy) under high temperature (120 °C, 8 min; 50 °C, 2 min; 180 °C, 10 min) and high pressure. Finally, element concentrations in lysates were measured according to the standard operating procedure using inductively coupled plasma mass spectrometry (ICP-MS) at the Korean Basic Science Institute (Supple 2A), and ion concentrations in lysates were evaluated using Inductively Coupled Plasma-Optical Emission Spectrometer (ICP-OES, OPTIMA 5300DV, PerkinElmer, USA) at Center for Materials Characterization and Machining, Ajou University (Supple 2B).

2.5. Histopathological analysis

A part of the brain, lung (right), heart, liver (right lobe), and spleen and a right kidney were fixed with 10% neutral buffered formalin, and a right testis was fixed in Bouin's solution. All processes for the histopathological analysis were performed according to the standard operating procedures of the Korea Institute of Toxicology (Daejeon, Korea).

2.6. LDH assay

The level of LDH released into the blood was measured using commercially available LDH assay kits (Biovision, CA, USA) according to the manufacturer's instructions. Briefly, sera (10 μL) were reacted with the LDH solution (200 μL) for 30 min at RT, and the absorbance at 450 nm was measured using a microplate spectrophotometer (Molecular Devices, Sunnyvale, CA, USA).

2.7. Cytokine assay

The concentration of interleukine (IL)-6 and IL-8 were determined using commercially available enzyme-linked immunosorbent assay kits (eBioscience, San Diego, CA, USA) according to the manufacturer's instructions. Finally, the reactions were stopped by adding 1 M H_3PO_4, and the absorbance at 450 nm was measured

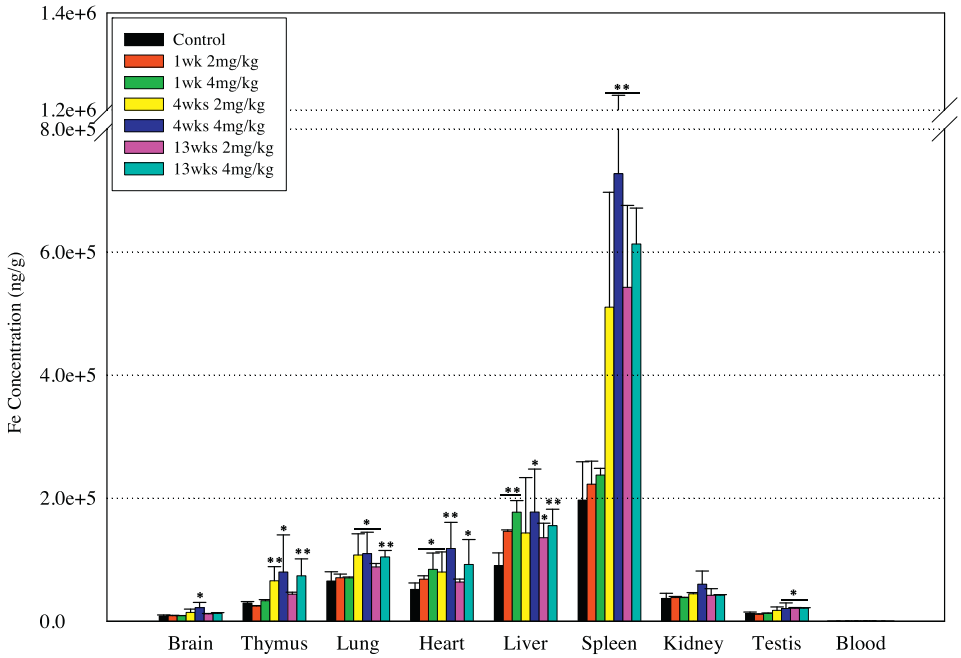

Fig. 2. Tissue distribution of M-FeNPs injected intravenously. Tissues were harvested at designated time points (control group: 4 mice/time point, treated group: 8 mice/group), and were digested in a mixture of HNO_3 (70%, 7 ml) and H_2O_2 (35%, 1 ml) solution using a microwave digestion system. Then, two lysates (three lysates for the control group) were pooled equivalently to make one sample for analysis ($n = 4$). Values are the mean ± SD for each group. $^*p < 0.05$; $^{**}p < 0.01$.

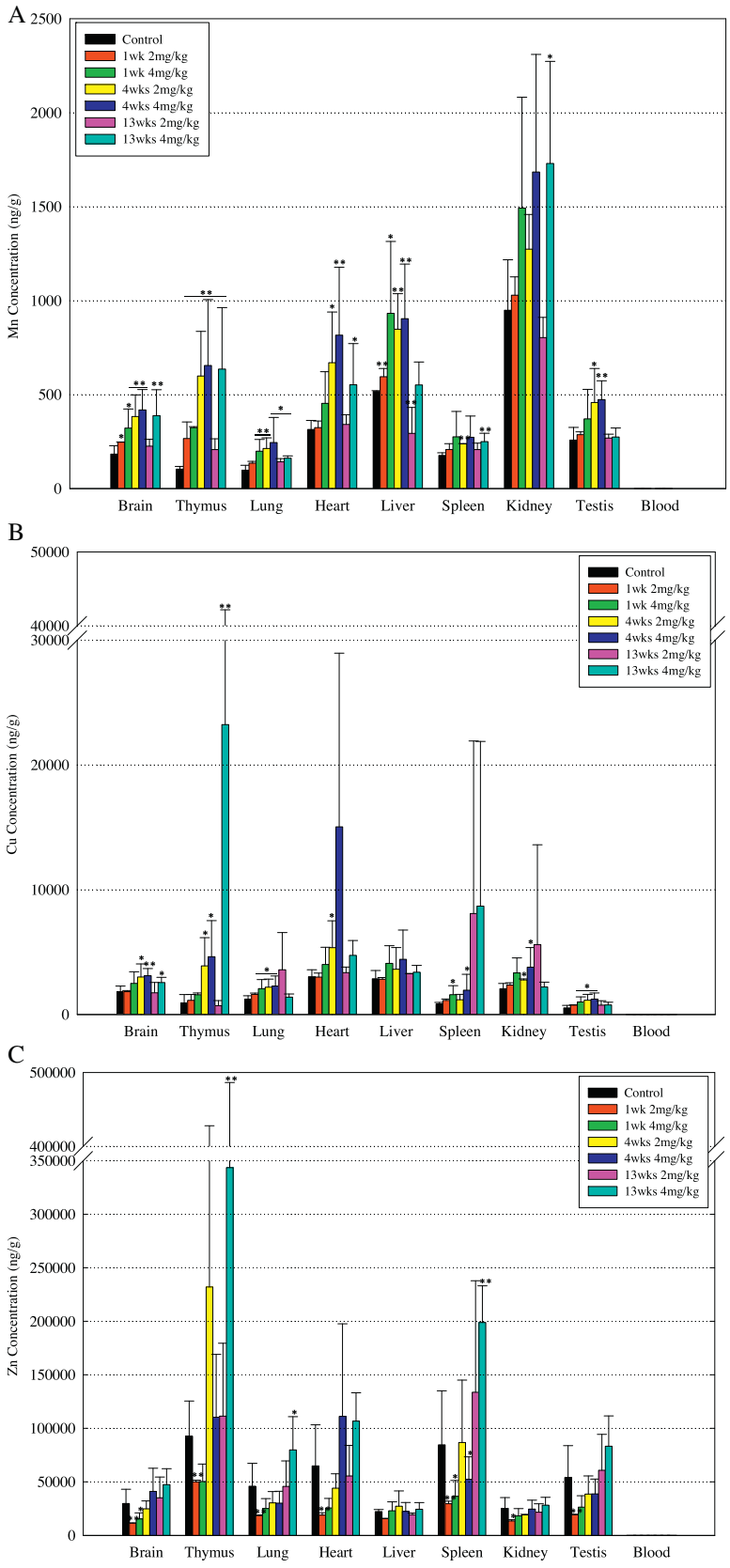

Fig. 3. Effect of M-FeNPs accumulation on homeostasis of redox reaction-related elements. Element concentrations in lysates were measured using ICP-MS ($n = 4$) and values show the mean ± SD for each group. (A) Mn, (B) Cu, and (C) Zn. $^{*}p < 0.05$; $^{**}p < 0.01$.

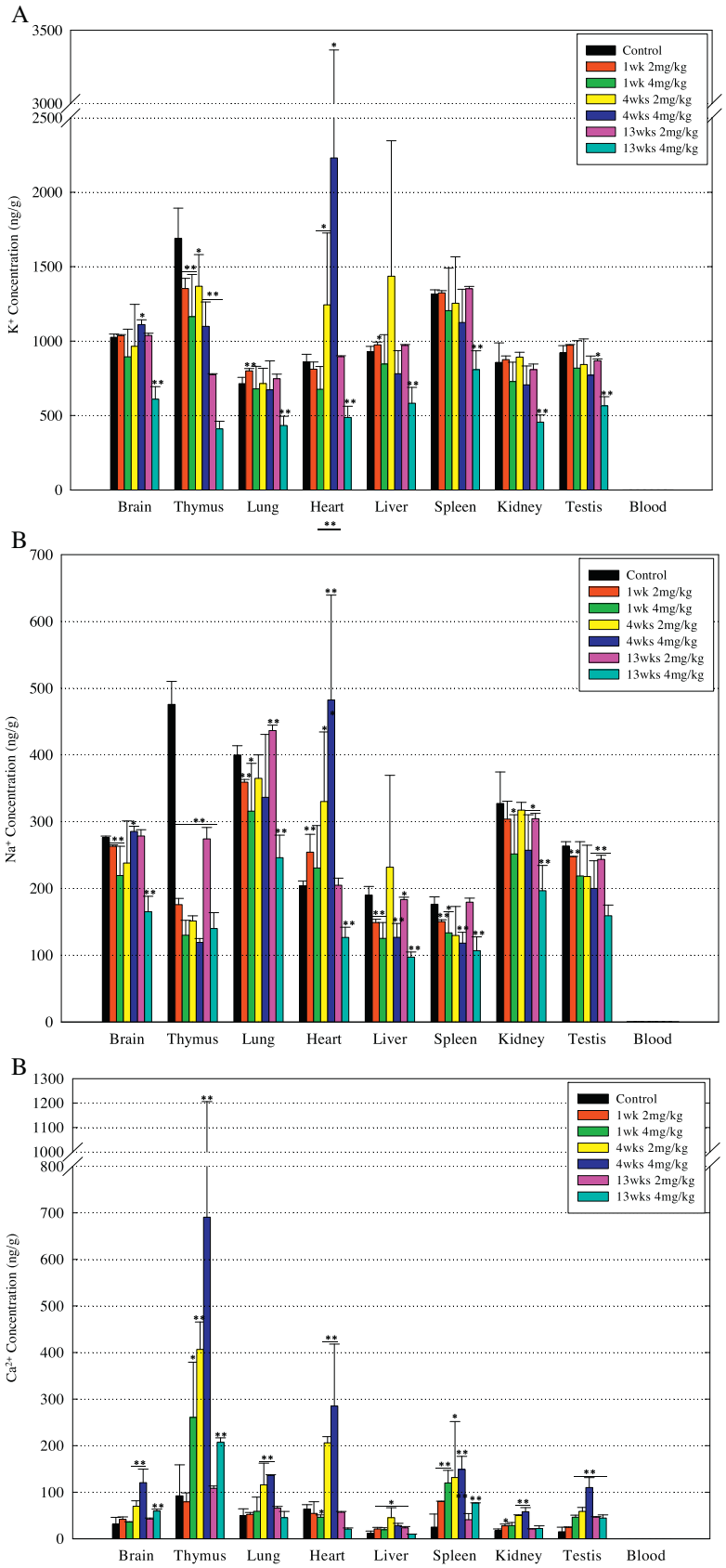

Fig. 4. Effects of M-FeNPs accumulation on the ion homeostasis. Ion concentrations in lysates were evaluated using ICP-OES ($n = 4$) and values are the mean ± SD for each group. (A) K^+, (B) Na^+, and (C) Ca^{2+}. *$p < 0.05$; **$p < 0.01$.

using an ELISA reader (Molecular Devices). The concentration of each cytokine was calculated from the linear portion of the standard curve that was generated under the same condition.

2.8. Immunophenotyping analysis

Splenocytes were made from spleen, which collected at designated time points after a single injection. Briefly, spleens were ground in RPMI media containing fetal bovine serum (2%) and washed once with PBS. After removing RBC with FACS lysis buffer, splenocytes were filtered using a 70 μm-pore size nylonmesh, and then were resuspended in FACS buffer. After blocking with Fc-block antibody to reduce nonspecific binding, splenocytes were incubated with the fluorescence dye labeled-corresponding fluorescence antibody (: phycoerythrin (PE)-CD11b, fluorescein isothiocyanate (FITC)-CD11c, allophycocyanin (APC)-MHC Class II (I-A/I-E), FITC-CD3e (for T cells), PE-CD19 (for B cells), APC-DX5 (NK cells), PE-CD4, FITC-CD8a, APC-CD40, peridinin chlorophyll protein-CD195, PE-CD123 (eBioscience); APC-CD86 (B7-2, BioLegend, Inc. San Diego, CA, USA); APC-CXCR2 (R&D Systems, Inc. Minneapolis, MN, USA)) for 30 min at 4 °C according to the manufacturer's instructions. Then, cells were washed twice with FACS buffer and analyzed on a FACSCalibur (BD Biosciences) flow cytometer with CellQuest software.

2.9. Statistical analysis

Data are the mean ± standard deviation (SD) for each group. Statistical analysis were performed for all the results, except histopathological changese and assessed difference between M-FeNPs-treated groups and the control group using Student's *t*-test (Graphpad Software, San Diego, CA, USA) and one way ANOVA test followed by Tukey's post hoc pairwise comparison. Asterisks ($^{*}p < 0.05$ and $^{**}p < 0.01$) indicate statistically significant differences to the control group.

3. Results

3.1. Effects on iron levels in tissues

The iron level in tissues reached the highest at 4 weeks after a single injection, and this elevation was maintained until 13 weeks post-injection (Fig. 2). M-FeNPs were primarily distributed in the liver at 1 week post-injection, and iron levels increased remarkably in the thymus, lung, heart, liver, and spleen at 4 weeks post-injection. Meanwhile, on 13 weeks post-injection, iron level were the highest in the spleen.

3.2. Effect on homeostasis of trace elements in tissues

As shown in Fig. 3, levels of redox reaction-related elements were significantly altered in tissues since 1 week post-injection. The levels of manganese (Mn, Fig. 3A) and copper (Cu, Fig. 3B) in tissues reached their maximum at 4 weeks post-injection, whereas the level of zinc (Zn, Fig. 3C) was down-regulated until 4 weeks post-injection, and then increased with time.

Table 1
Hematological changes following M-FeNPs accumulation. Blood (control group: 4 mice/time point, $n = 12$; treated group: 8 mice/group, $n = 8$) was collected at designated time points after a single intravenous injection of M-FeNPs. Values are the mean ± SD for each group. $^{*}p < 0.05$; $^{**}p < 0.01$.

		WBC (K/μL)	LYM (%)	MONO (%)	NEU (%)	EOS (%)	BASO (%)	RBC (M/mm^3)	MCV (fL)	HCT (%)	MCH (pg)	MCHC (g/dL)	HGB (g/dL)	RDW (%)	PLT (K/μL)	MPV (fL)
Control		1.9 ± 0.3	86.3 ± 2.0	3.8 ± 1.4	4.7 ± 0.8	0.4 ± 0.2	0.6 ± 0.2	6.9 ± 0.6	64.3 ± 2.5	44.2 ± 2.4	18.3 ± 1.6	28.6 ± 3.3	12.7 ± 2.1	15.3 ± 0.9	1132.0 ± 173.0	6.0 ± 0.4
1 wks	2 mg/kg	5.7 ± 2.5**	91.9 ± 0.9*	2.0 ± 0.1**	5.2 ± 0.5	0.4 ± 0.3	0.6 ± 0.1	7.1 ± 0.1	57.8 ± 0.6**	41.1 ± 0.7*	17.0 ± 0.1	29.3 ± 0.5	12.1 ± 0.0	16.7 ± 0.1	1127.0 ± 18.8	5.8 ± 0.3
	4 mg/kg	7.4 ± 0.4**	90.8 ± 1.3*	2.0 ± 0.4*	4.6 ± 1.9	1.6 ± 2.6	0.4 ± 0.1	6.9 ± 0.4	58.2 ± 2.6*	40.2 ± 3.6	17.0 ± 0.9	29.1 ± 1.4	11.7 ± 1.2	16.5 ± 0.4	1189.2 ± 246.4	5.7 ± 0.2
4 wks	2 mg/kg	5.5 ± 1.1**	87.8 ± 6.3	2.0 ± 0.4*	9.4 ± 6.6	0.3 ± 0.3	0.5 ± 0.3	7.3 ± 0.7	53.6 ± 3.4**	38.5 ± 2.9*	16.8 ± 0.7	31.1 ± 0.9	12.0 ± 0.9	16.9 ± 0.6	999.8 ± 362.9	6.0 ± 0.5
	4 mg/kg	6.9 ± 3.1**	89.0 ± 2.3	2.8 ± 0.6*	6.5 ± 0.7**	1.0 ± 1.3	0.7 ± 0.1	7.3 ± 0.3	55.2 ± 3.7**	40.2 ± 1.6*	16.3 ± 0.3*	29.5 ± 2.0	11.9 ± 0.7	16.4 ± 0.8	924.3 ± 184.7	5.8 ± 0.3
13 wks	2 mg/kg	1.9 ± 0.9	53.0 ± 9.9**	3.1 ± 1.4	42.7 ± 8.0**	0.9 ± 0.2**	0.2 ± 0.1	9.1 ± 0.2**	57.2 ± 0.8**	49.6 ± 1.0**	15.5 ± 0.3**	27.6 ± 0.4	13.7 ± 0.8	14.7 ± 0.2	1486.0 ± 123.1*	6.4 ± 0.4
	4 mg/kg	2.9 ± 1.4	62.6 ± 5.5**	3.1 ± 1.1	32.5 ± 5.5**	1.4 ± 0.2**	0.2 ± 0.1	9.4 ± 0.6**	56.9 ± 1.6**	52.7 ± 1.0**	15.4 ± 0.6**	27.3 ± 0.6	14.4 ± 0.2	14.6 ± 0.7	1510.2 ± 66.5**	5.6 ± 0.2

3.3. Effect on the ion environment in tissues

To identify the effect on the ion environment in tissues, in this study, we measured levels of three cations, including potassium (K^+), sodium (Na^+), and calcium (Ca^{2+}). While the levels of K^+ (Fig. 4A) and Na^+ (Fig. 4B) in tissue tended to decrease with time, as compared to the control, those of Ca^{2+} (Fig. 4C) increased into the maximum at 4 weeks post-injection. Notably, the elevation of Ca^{2+} level in brain, thymus, spleen, and testis, remained until 13 weeks after injection.

3.4. Effects on physiology and histopathology

The number of white blood cells (WBCs) was significantly elevated in the treated groups compared to the control until 4 weeks after injection (Table 1). While the percentage of lymphocytes in WBCs increased at 1 week after injection compared to the control, the percentage of neutrophils increased since 4 weeks (4 mg/kg). Noteworthy, on 13 weeks after injection, while the percentage of lymphocytes clearly decreased in the treated groups as compared to the control, the percentages of neutrophils and eosinophils notably increased. More interestingly, levels of RBC and hematocrit (HCT) and the platelet (PLT) number were significantly elevated in the treated groups compared to the control. Additionally, as compared to the control, while LDH level reached the maximum at 1 week after injection (Fig. 5A), IL-8 secretion tended to increase with time in the treated groups (Fig. 5B). Meanwhile, IL-6 secretion was significantly enhanced at 4 mg/kg dose only compared to the control. Subsequently, pigmented macrophages were clearly observed in the spleen and lung of the treated groups compared to the control (Fig. 6), however, there were no remarkable pathological changes following accumulation of M-FeNPs.

3.5. Effects on the expression of immune response-related surface markers

While the T cell population was dominant in lymphocytes of the treated groups at 1 week after injection as compared to the control, the B cell population rapidly increased at 4 and 13 weeks post-injection (Fig. 7A). The expression of antigen presentation related-proteins, including CD80, CD86, MHC class II, and CD40, was also notably attenuated in the treated group compared to the control at all the time points, which was accompanied by a decrease in the population of maturated dendritic cells (Fig. 7B). On the other hand, as compared to the control, the expression of several chemokines, including CXCR2, CD195, and CD123, was enhanced on the splenocytes of the treated groups (Fig. 7C).

4. Discussion

Owing to the accumulating investments and efforts for applications of nanoparticles in food products, drug delivery systems, medical devices, and consumer products, direct and indirect human exposures to nanoparticles are expected to increase rapidly in the near future with concern about the adverse effect on environment and human (Bhirde et al., 2011; Hood, 2004; Liu and Lai, 2015; Liu et al., 2013; Smlkova et al., 2015). The OECD listed a set of endpoints to take into account for phase one testing, including nanomaterial identification, characterization, environmental fate, and mammalian and environmental toxicology. Toxicokinetics is one of the most important endpoints with respect to mammalian toxicology because the toxicity of nanoparticles depends on not only the external dose but also the internal dose. The functional coating of nanoparticles is an important factor determining their kinetics and toxicity. For example, quantum dots (QDs) coated with a short peptide chain were distributed to the lymph nodes, liver, and bone marrow within 1 h after injection, whereas long-chain surface coated QDs remained in the circulation for at least 3 days (Ballou et al., 2004). Additionally, although they enter the body via different ports, nanoparticles can circulate through the body systemically via the lymphatic system and the bloodstream, either freely or after being phagocytosed, they can also penetrate into RBC (Geiser et al., 2005; Moghimi et al., 2001; Rothen-Rutishauser et al., 2006). In this study, M-FeNPs were coated with phospholipid, a major component of cell membranes, and were found to accumulate the most in

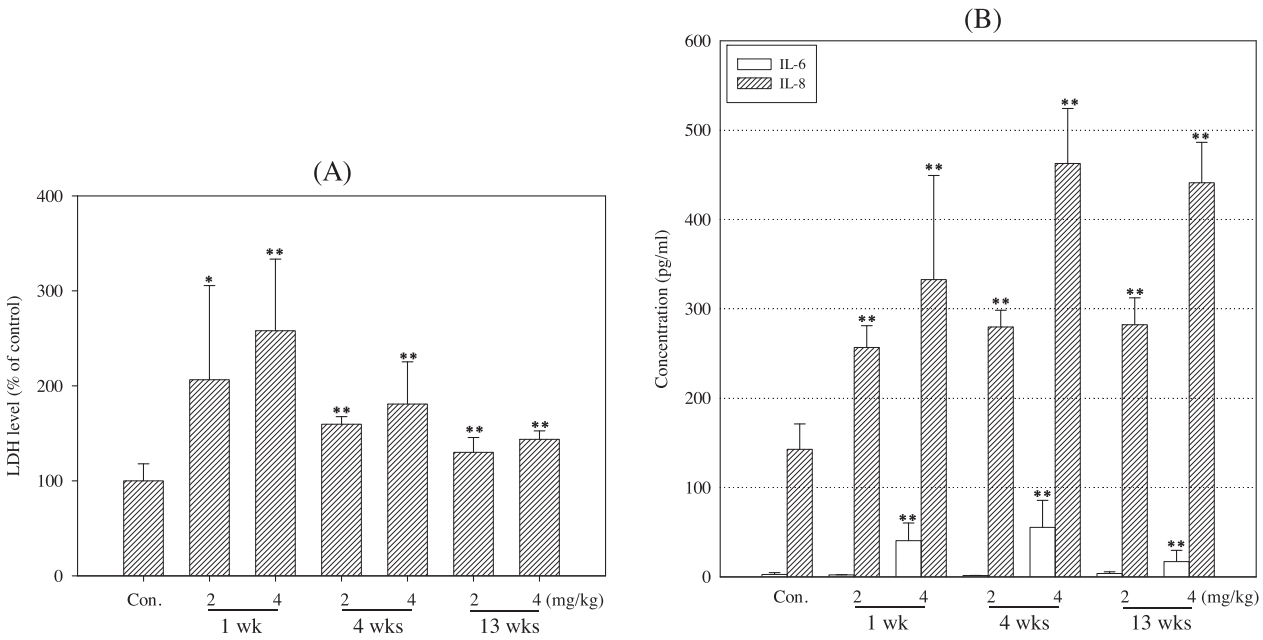

Fig. 5. Physiological changes following accumulation of M-FeNPs. A part of blood (600 μL, control group: $n = 12$, treated group; $n = 8$) was centrifuged to make serum for cytokine analysis and LDH assay. Data are the mean ± SD for each group.*$p < 0.05$; **$p < 0.01$. (A) LDH release. Sera (10 μL) were reacted with the LDH solution (200 μL) for 30 min at room temperature, and the absorbance value was measured three times with interval of 10 min (B) cytokine secretion. The cytokine levels were calculated using standard curve, which was made under the same condition. (0–1000 pg/mL).

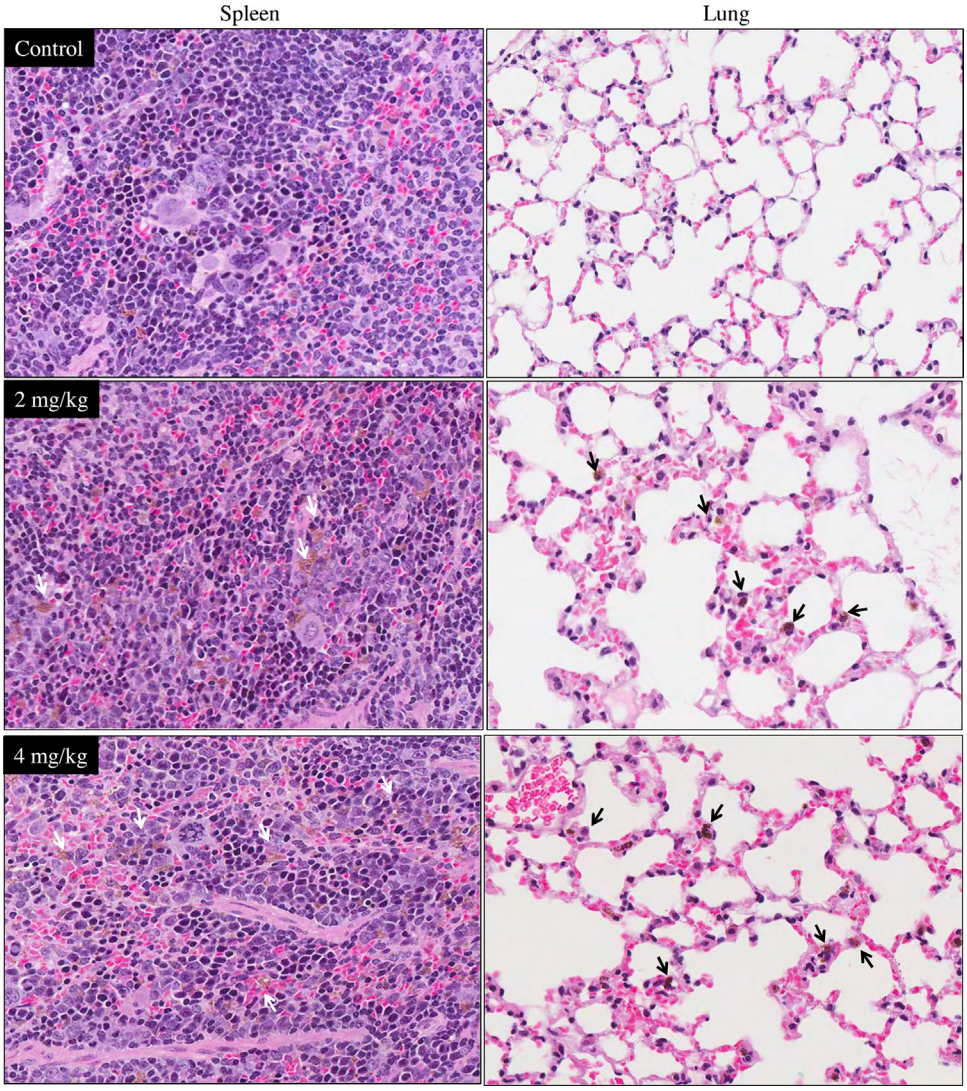

Fig. 6. Histopathological changes following accumulation of M-FeNPs. Tissues (4 samples/group) were harvested at 1, 4, and 13 weeks after a single intravenous injection. Representive images by dose on 13 weeks post-exposure were provided.

the spleen at 13 weeks after a single injection. Considering that very little ingested Fe was excreted outside the body, except during menstruation (Morgan and Oates, 2002; Oates et al., 2000), and that M-FeNPs existed side by side with membrane of organelle within macrophage cells (Park et al., 2014a; Park et al., 2014b), we can expect that M-FeNPs may be removed outside the body via the spleen with dead cells and be accumulated in the spleen with dead RBC.

Excess iron can generate free radicals in a biological system, which is followed by oxidative stress, and these radicals can be removed through redox reaction (Luo et al., 2015; Park et al., 2014a; Periasamy et al., 2014; Sun et al., 2011; Wang et al., 2009). In this process, the tissue levels of Cu, Mn, and Zn, components of superoxide dismutase, an antioxidant, can be altered (Park et al., 2014c). Additionally, many trace elements exist as divalent ions in the body, thus, the absorption of an element can influence the absorption of other elements by binding competitively to a cell membrane receptor. Moreover, generation of free radicals is not only feasible translocation of nanoparticles into other tissues through membrane damage, but can also initiate an inflammatory response in the body. As expected, the accumulation of Fe significantly altered the levels of Cu, Mn, and Zn in all the tissues evaluated in this study and increased the level of LDH release into the blood accompanying the elevated secretion of a pro-inflammatory cytokine (IL-6) and a chemokine (IL-8).

Redox reactions involve the transfer of electrons and higher organisms require a subtle electrolyte balance between the intracellular and extracellular environments (Chen et al., 2011; Liu et al., 2009; Liu et al., 2011). In particular, the tight regulation of osmotic pressure is essential to maintain normally physiological events, such as the hydration of the body, blood pH, and nervous and muscle function. In addition, the movement of ions across the membranes of cells and organelles is mediated by several types of transport protein, and the rate and extent of ion transport across membranes are influenced by not only the ion concentrations on the two sides of the membrane but also the voltage that exists across the membrane. Growing evidences suggested that nanoparticles can penetrate the cell membrane by electrostatic power or via ion channels, and the intracellular ion environment could be altered following exposure to nanoparticles. For example, QDs induced cell death via elevation of the cytoplasmic Ca^{2+} level and impairment of Na^{+} channel function (Tang et al., 2008), and tungsten carbide nanoparticles caused potential neurotoxicity by inhibiting voltage-gated K^{+} currents of hippocampal CA1 neurons (Shan et al., 2012). In addition, K^{+} channel blockers, such as tetraethylammonium, 4-amino pyridine, and margatoxin, reduced

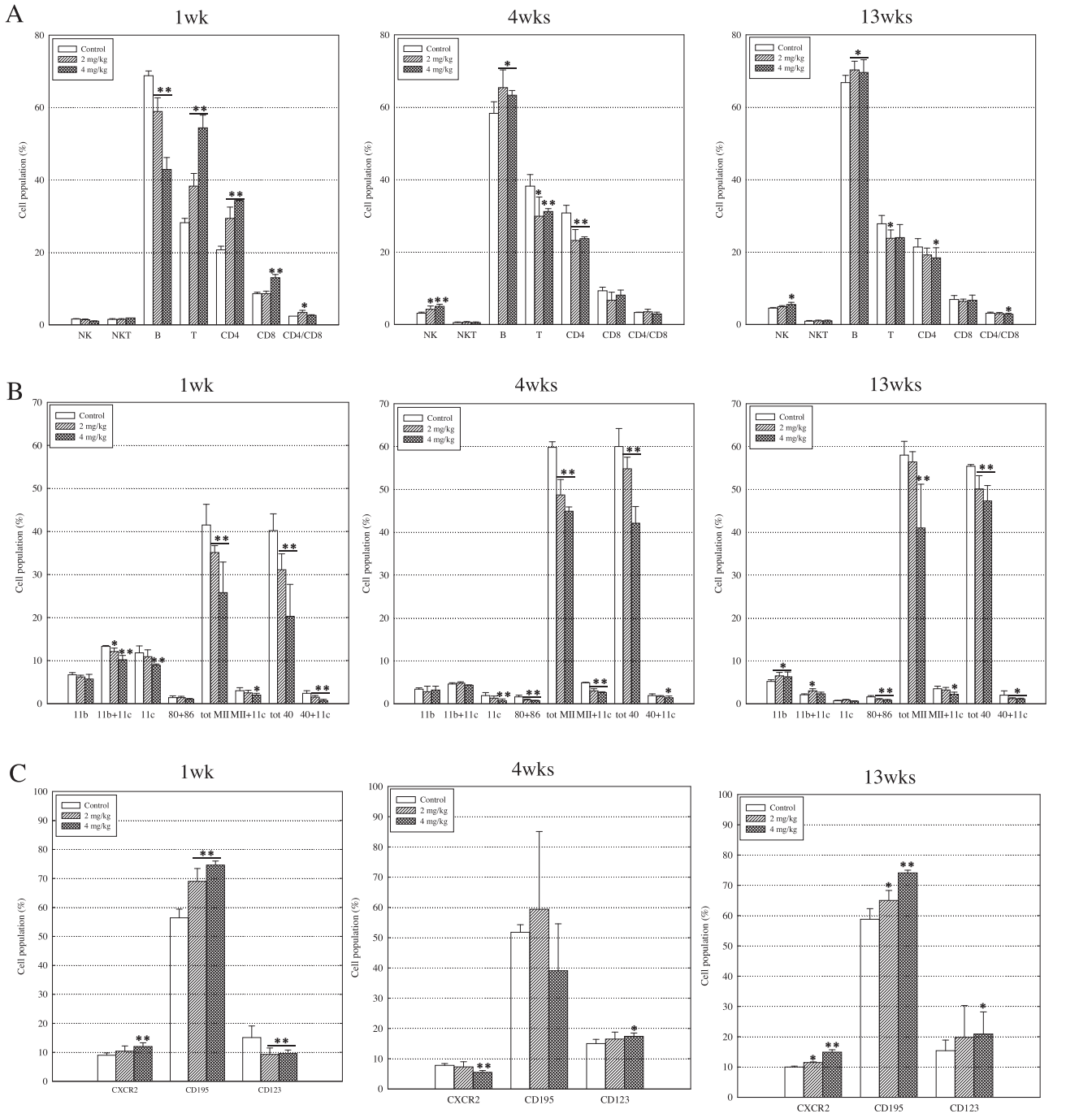

Fig. 7. Effect of M-FeNPs accumulation on expression of immune response-related surface makers. After blocking with Fc-block antibody (CD16), splenocytes (4 samples/group) were stained in the dark with directly conjugated monoclonal antibodies for 30 min at 4 °C. 10,000 cells per sample were counted. The results were expressed as the mean ± SD. $^{*}p < 0.05$; $^{**}p < 0.01$. (A) Distribution of lymphocyte components, (B) Expression of antigen presentation-related surface markers, tot: total, MII: MHC class II, 11b (CD11b+/CD11c-): regular dendritic cells, 11b + 11c (CD11b+/CD11c+): immature dendritic cells, 11c (CD11b-/CD11c+): mature dendritic cells, 80 + 86: CD80+/CD86+, 40: CD40 (C) Expression of chemotaxis-related surface markers.

silica nanoparticle-induced cytotoxicity and inflammation by blocking K^+ efflux induced by outward K^+ channel activation (Yang et al., 2013). Moreover, silver nanoparticles decreased the peak amplitude and overshoot of the evoked single action potential and increased half-width in experiments using whole cell current-clamp recordings. This means that silver nanoparticles may alter the action potential of hippocampal CA1 neurons by depressing the voltage-gated Na^+ current (Liu et al., 2009). In the current study, we measured tissue levels of Na^+, K^+, and Ca^{2+}, which are the primary ions in terms of electrophysiology. Interestingly, levels of Na^+ and K^+ tended to decrease in all tissues examined, whereas Ca^{2+} accumulated notably in these tissues on 4 weeks after injection. In particular, the Ca^{2+} levels in the brain and testes were elevated until 13 weeks after a single injection. We believe that further research is needed to elucidate the detailed mechanism, although our results were worthy in reporting the electrophysiological changes occurring following exposure to nanoparticles in vivo.

As reported above, M-FeNPs were mainly distributed in the spleen, a primary lymphoid organ, at 13 weeks after the single injection. Additionally, accumulating evidence suggests that nanoparticles can influence adaptive immunity, especially by affecting the function of antigen presenting cells (Jiménez-Periáñez et al., 2013;

Tkach et al., 2013; Uto et al., 2012). Considering that adaptive immunity is stimulated 4 to 7 days after a foreign body enters the body, and that antigen presenting cells, including dendritic cells, macrophages, and B cells, are key players in adaptive immunity, in a follow-up study, we examined changes in the expression of surface markers on splenocytes over time (Kindt et al., 2006). At 13 weeks post-injection, B cells had become dominant among the lymphocytes, and maturation (CD11b-/CD11c+) of dendritic cells, but not formation of immature dendritic cells (CD11b+/CD11c+), was impaired. While expression of antigen presentation-related proteins such as CD80, CD86, MHC class II, and CD40 was attenuated on the surface of splenocytes, the expression of chemokine receptors, including CD195, CXCR2, and CD123, was enhanced. Additionally, these results accompanied an increased secretion of IL-6 and IL-8 and an elevated percentage of neutrophils in blood lymphocytes. CXCR2, as a receptor for CXC chemokines, was expressed on the surface of neutrophils and binds to IL-8 (Kindt et al., 2006; Pease and Sabroe, 2002). CCR5 (CD195), a CC chemokine receptor, is predominantly expressed on the surface of T cells, macrophages, dendritic cells, and eosinophils, and binds to RANTES and MIP-1 alpha and beta (de Oliveira et al., 2014; Mueller and Strange 2004). In addition, CD123 is found on pluripotent progenitor cells and is a receptor for IL-3, which stimulates both the differentiation of multipotent hematopoietic stem cells into myeloid progenitor cells and the proliferation of all cells in the myeloid lineage (granulocytes, monocytes, and dendritic cells), in combination with other cytokines such as GM-CSF and IL-6 (Liu et al., 2015). We are continuously exposed to foreign bodies, and adaptive immunity is initiated by antigen processing by phagocytic cells. Therefore, suppression of antigen presentation function following accumulation of M-FeNPs in the spleen can ultimately influence the defensive abilities of our immune system.

Taken together, we suggest that accumulation of intravenously injected M-FeNPs may induce adverse health effects by disturbing homeostasis of the immune regulation and ion environment.

Conflict of interest

The authors report no declarations of interest.

Acknowledgement

This work was supported by the Basic Science Research Program through the National Research Foundation of Korea funded by the Ministry of Education, Science and Technology (2011-35B-E00011).

Appendix A. Supplementary data

Supplementary data associated with this article can be found, in the online version, at http://dx.doi.org/10.1016/j.toxlet.2015.11.030.

References

Altaf, H., Revell, P.A., 2013. Evidence for active antigen presentation by monocyte/macrophages in response to stimulation with particles: the expression of NFkB transcription factors and costimulatory molecules. Inflammopharmacology 21 (4), 279–290.
Antonelli, A., Sfara, C., Battistelli, S., Canonico, B., Arcangeletti, M., Manuali, E., Salamida, S., Papa, S., Magnani, M., 2013. New strategies to prolong the in vivo life span of iron-based contrast agents for MRI. PLoS One 8 (10), e78542.
Ballou, B., Lagerholm, B.C., Ernst, L.A., Bruchez, M.P., Waggoner, A.S., 2004. Noninvasive imaging of quantum dots in mice. Bioconjug. Chem. 15 (1), 79–86.
Baratli, Y., Charles, A.L., Wollff, V., Ben Tahar, L., Smiri, L., Bouitbir, J., Zoll, J., Sakly, M., Auger, C., Vogel, T., Abdelmelek, H., Tebourbi, O., Geny, B., 2014. Age modulates Fe3O4 nanoparticles liver toxicity: dose-dependent decrease in mitochondrial respiratory chain complexes activities and coupling in middle-aged as compared to young rats. Biomed. Res. Int. 2014, 474081.
Bhirde, A., Xie, J., Swierczewska, M., Chen, X., 2011. Nanoparticles for cell labeling. Nanoscale 3 (1), 142–153.
Braakhuis, H.M., Gosens, I., Krystek, P., Boere, J., Cassee, F.R., Fokkens, P., Post, J., van Loveren, H., Park, M., 2014. Particle size dependent deposition and pulmonary inflammation after short-term inhalation of silver nanoparticles. Part. Fibre Toxicol. 11 (1) 49.
Chen, E.Y., Gamica, M., Wang, Y.C., Chen, C.S., Chin, W.C., 2011. Mucin secretion induced by titanium dioxide nanoparticles. PLoS One 6 (1), e16198.
Fabian, E., Landsiedel, R., Ma-Hock, L., Wiench, K., Wohlleben, W., van Ravenzwaay, B., 2008. Tissue distribution and toxicity of intravenously administered titanium dioxide nanoparticles in rats. Arch. Toxicol. 82 (3), 151–157.
Fraga, S., Brandão, A., Soares, M.E., Morais, T., Duarte, J.A., Pereira, L., Soares, L., Neves, C., Pereira, E., Bastos Mde, L., Carmo, H., 2014. Short- and long-term distribution and toxicity of gold nanoparticles in the rat after a single-dose intravenous administration. Nanomedicine 10 (8), 1757–1766.
Fujihara, J., Tongu, M., Hashimoto, H., Yamada, T., Kimura-Kataoka, K., Yasuda, T., Fujita, Y., Takeshita, H., 2015. Distribution and toxicity evaluation of ZnO dispersion nanoparticles in single intravenously exposed mice. J. Med. Investig. 62 (1–2), 45–50.
Geiser, M., Rothen-Rutishauser, B., Kapp, N., Schürch, S., Kreyling, W., Schulz, H., Semmler, M., Im Hof, V., Heyder, J., Gehr, P., 2005. Ultrafine particles cross cellular membranes by nonphagocytic mechanisms in lungs and in cultured cells. Environ. Health Perspect. 113 (11), 1555–1560.
Hagens, W.I., Oomen, A.G., de Jong, W.H., Cassee, F.R., Sips, A.J., 2007. What do we (need to) know about the kinetic properties of nanoparticles in the body? Regul. Toxicol. Pharmacol. 49 (3), 217–229.
Hilger, I., Kaiser, W.A., 2012. Iron oxide-based nanostructures for MRI and magnetic hyperthermia. Nanomedicine (London) 7 (9), 1443–1459.
Hood, E., 2004. Nanotechnology: looking as we leap. Environ. Health Perspect. 112 (13), A740–749.
Jiménez-Periáñez, A., Abos Gracia, B., López Relaño, J., Diez-Rivero, C.M., Reche, P.A., Martínez-Naves, E., Matveveva, E., Gómez del Moral, M., 2013. Mesoporous silicon microparticles enhance MHC class I cross-antigen presentation by human dendritic cells. Clin. Dev. Immunol. 362163.
Kindt, T.J., Osborne, B.A., Goldsby, R.A., 2006. Kuby Immunology, 6th ed. W.H. Freeman & Company.
Liu, R., Lai, R., 2015. Potentials of engineered nanoparticles as fertilizers for increasing agronomic productions. Sci. Total Environ. 514, 131–139.
Liu, G., Men, P., Harris, P.L., Rolston, R.K., Perry, G., Smith, M.A., 2006. Nanoparticle iron chelators: a new therapeutic approach in Alzheimer disease and other neurologic disorders associated with trace metal imbalance. Neurosci. Lett. 406 (3), 189–193.
Liu, Z., Ren, G., Zhang, T., Yang, Z., 2009. Action potential changes associated with the inhibitory effects on voltage-gated sodium current of hippocampal CA1 neurons by silver nanoparticles. Toxicology 264 (3), 179–184.
Liu, Z., Liu, S., Ren, G., Zhang, T., Yang, Z., 2011. Nano-CuO inhibited voltage-gated sodium current of hippocampal CA1 neurons via reactive oxygen species but independent from G-proteins pathway. J. Appl. Toxicol. 31 (5), 439–445.
Liu, G., Gao, J., Ai, H., Chen, X., 2013. Applications and potential toxicity of magnetic iron oxide nanoparticles. Small 9 (9–10), 1533–1545.
Liu, K., Zhu, M., Huang, Y., Wei, S., Xie, J., Xiao, Y., 2015. CD123 and its potential clinical application in leukemias. Life Sci. 122, 59–64.
Luo, C., Li, Y., Yang, L., Wang, X., Long, J., Liu, J., 2015. Superparamagnetic iron oxide nanoparticles exacerbate the risks of reactive oxygen species-mediated external stresses. Arch. Toxicol. 89 (3), 357–369.
Moghimi, S.M., Hunter, A.C., Murray, J.C., 2001. Long-circulating and target-specific nanoparticles: theory to practice. Pharmacol. Rev. 53 (2), 283–318.
Monopoli, M.P., Aberg, C., Salvati, A., Dawson, K.A., 2012. Biomolecular coronas provide the biological identity of nanosized materials. Nat. Nanotechnol. 7 (12), 779–786.
Morgan, E.H., Oates, P.S., 2002. Mechanisms and regulation of intestinal iron absorption. Blood Cells Mol. Dis. 29 (3), 384–399.
Mueller, A., Strange, P.G., 2004. The chemokine receptor, CCR5. Int. J. Biochem. Cell Biol. 36 (1), 35–38.
Nel, A.E., Mädler, L., Veleqol, D., Xia, T., Hoek, E.M., Somasundaran, P., Klaessig, F., Castranova, V., Thompson, M., 2009. Understanding biophysicochemical interactions at the nano-bio interface. Nat. Mater. 8 (7), 543–557.
Oates, P.S., Jeffrey, G.P., Basclain, K.A., Thomas, C., Morgan, E.H., 2000. Iron excretion in iron-overloaded rats following the change from an iron-loaded to an iron-deficient diet. J. Gastroenterol. Hepatol. 15 (6), 665–674.
Oberdörster, G., Oberdörster, E., Oberdörster, J., 2005. Nanotoxicology: an emerging discipline evolving from studies of ultrafine particles. Environ. Health Perspect. 113 (7), 823–839.
Park, J., An, K., Hwang, Y., Park, J.G., Noh, H.J., Kim, J.Y., Park, J.H., Hwang, N.M., Hyeon, T., 2004. Ultra-large-sacle syntheses of monodisperse nanocrystals. Nat. Mater. 3, 891–895.
Park, E.J., Choi, D.H., Kim, Y., Lee, E.W., Song, J., Cho, M.H., Kim, J.H., Kim, S.W., 2014a. Magnetic iron oxide nanoparticles induce autophagy preceding apoptosis through mitochondrial damage and ER stress in RAW264.7 cells. Toxicol. In Vitro 28 (8), 1402–1412.
Park, E.J., Umh, H.N., Choi, D.H., Cho, M.H., Choi, W., Kim, S.W., Kim, Y., Kim, J.H., 2014b. Magnetite- and maghemite-induced different toxicity in murine alveolar macrophage cells. Arch. Toxicol. 88 (8), 1607–1618.
Park, E.J., Lee, G.H., Yoon Ch Kang, M.S., Kim, S.N., Cho, M.H., Kim, J.H., Kim, D.W., 2014c. Time-dependent bioaccumulation of distinct rod-type TiO_2

nanoparticles: comparison by crystalline phase. J. Appl. Toxicol. 34 (11), 1265–1270.
Park, E.J., Oh, S.Y., Lee, S.J., Lee, K., Kim, Y., Lee, B.S., Kim, J.S., 2015. Chronic pulmonary accumulation of iron oxide nanoparticles induced Th1-type immune response stimulating the function of antigen-presenting cells. Environ. Res. 143 (Pt. A), 138–147.
Pease, J.E., Sabroe, I., 2002. The role of interleukin-8 and its receptors in inflammatory lung disease: implications for therapy. Am. J. Respir. Med. 2 (1), 19–25.
Periasamy, V.S., Athinarayanan, J., Alhazmi, M., Alatiah, K.A., Alshatwi, A.A., 2014. Fe_3O_4 nanoparticle redox system modulation via cell-cycle progression and gene expression in human mesenchymal stem cells. Environ. Toxicol. (Epub ahead of print).
Rosen, J.E., Chan, L., Shieh, D.B., Gu, F.X., 2012. Iron oxide nanoparticles for targeted cancer imaging and diagnostics. Nanomedicine 8 (3), 275–290.
Rothen-Rutishauser, B.M., Schürch, S., Haenni, B., Kapp, N., Gehr, P., 2006. Interaction of fine particles and nanoparticles with red blood cells visualized with advanced microscopic techniques. Environ. Sci. Technol. 40 (14), 4353–4359.
Sayes, C.M., Reed, K.L., Warheit, D.B., 2007. Assessing toxicity of fine and nanoparticles: comparing in vitro measurements to in vivo pulmonary toxicity profiles. Toxicol. Sci. 97 (1), 163–180.
Seydoux, E., Rothen-Rutishauser, B., Nita, I.M., Balog, S., Gazdhar, A., Stumbles, P.A., Petri-Fink, A., Blank, F., von Garnier, C., 2014. Size-dependent accumulation of particles in lysosomes modulates dendritic cell function through impaired antigen degradation. Int. J. Nanomed. 9, 3885–3902.
Shan, D., Xie, Y., Ren, G., Yang, Z., 2012. Inhibitory effect of tungsten carbide nanoparticles on voltage-gated potassium currents of hippocampal CA1 neurons. Toxicol. Lett. 209 (2), 129–135.
Shinohara, N., Danno, N., Ichinose, T., Sasaki, T., Fukui, H., Honda, K., Gamo, M., 2014. Tissue distribution and clearance of intravenously administered titanium dioxide (TiO_2) nanoparticles. Nanotoxicology 8 (2), 132–141.
Smlkova, B., El Yamani, N., Collins, A.R., Gutleb, A.C., Dusinska, M., 2015. Nanoparticles in food. Epigenetic changes induced by nanomaterials and possible impact on health. Food Chem. Toxicol. 77, 64–73.
Sun, J., Wang, S., Zhao, D., Hun, F.H., Weng, L., Liu, H., 2011. Cytotoxicity, permeability, and inflammation of metal oxide nanoparticles in human cardiac microvascular endothelial cells. Cell Biol. Toxicol. 27 (5), 333–342.
Tang, M., Xing, T., Zeng, J., Wang, H., Li, C., Yin, S., Yan, D., Deng, H., Liu, J., Wang, M., Chen, J., Ruan, D.Y., 2008. Unmodified CdSe quantum dots induce elevation of cytoplasmic calcium levels and impairment of functional properties of sodium channels in rat primary cultured hippocampal neurons. Environ. Health Perspect. 116 (7), 915–922.
Tkach, A.V., Yanamala, N., Stanley, S., Shurin, M.R., Shurin, G.V., Kisin, E.R., Murray, A. R., Pareso, S., Khaliullin, T., Kotchey, G.P., Castranova, V., Mathur, S., Fadeel, B., Star, A., Kagan, V.E., Shvedova, A.A., 2013. Graphene oxide, but not fullerenes, targets immunoproteasomes and suppresses antigen presentation by dendritic cells. Small 9 (9–10), 1686–1690.
Utembe, W., Potgieter, K., Stefaniak, A.B., Gulumian, M., 2015. Dissolution and biodurability: important parameters needed for risk assessment of nanomaterials. Part. Fibre Toxicol. 12 11.
Uto, T., Toyama, M., Nishi, Y., Akagi, T., Shima, F., Akashi, M., Baba, M., 2012. Uptake of biodegradable poly(γ-glutamic acid) nanoparticles and antigen presentation by dendritic cells in vivo. Results Immunol. 3, 1–9.
Velez, L.I., Delaney, K.A., 2006. Heavy metals: iron, lead, arsenic and mercury, In: Marx, J.A., Hockberger, R.S., Wallas, R.M., et al. (Eds.), Rosen's Emergency Medicine Concepts and Clinical Practice. 6th ed. Mosby, Philadelphia, Pennsylvania, pp. 2418–2451.
Wahajuddin, Arora, S., 2012. Superparamagnetic iron oxide nanoparticles: magnetic nanoplatforms as drug carriers. Int. J. Nanomed. 7, 3445–3471.
Wang, J.X., Fan, Y.B., Gao, Y., Hu, Q.H., Wang, T.C., 2009. TiO2 nanoparticles translocation and potential toxicological effect in rats after intraarticular injection. Biomaterials 30 (27), 4590–4600.
Wittmaack, K., 2007. In search of the most relevant parameter for quantifying lung inflammatory response to nanoparticle exposure: particle number, surface area, or what? Environ. Health Perspect. 115 (2), 187–194.
Yah, C.S., Simate, G.S., Iyuke, S.E., 2012. Nanoparticles toxicity and their routes of exposures. Pak. J. Pharm. Sci. 25 (2), 477–491.
Yang, L., Kuang, H., Zhang, W., Aguilar, Z.P., Xiong, Y., Lai, W., Xu, H., Wei, H., 2015. Size dependent biodistribution and toxicokinetics of iron oxide magnetic nanoparticles in mice. Nanoscale 7 (2), 625–636.
de Oliveira, C.E., Oda, J.M., Losi Guembarovski, R., de Oliveira, K.B., Ariza, C.B., Neto, J. S., Banin Hirata, B.K., Watanabe, M.A., 2014. CC chemokine receptor 5: the interface of host immunity and cancer. Dis. Markers 2014, 126954.
www.oecd.org, 2010. Environment directorate joint meeting of the chemicals committee and the working party on chemicals, pesticides and biotechnology. ENV/JM/MONO (2010); 46.
Yang, L., Yan, Q., Zhao, J., Li, J., Zong, X., Yang, L., Wang, Z., 2013. The role of potassium channel in silica nanoparticle-induced inflammatory effect in human vascular endothelial cells in vitro. Toxicol. Lett. 223 (1), 16–24.